Reactor Modeling and Recipe Optimization of Polyether Polyol Processes: Polypropylene Glycol

Yisu Nie and Lorenz T. Biegler
Dept. of Chemical Engineering, Carnegie Mellon University, Pittsburgh, PA 15213

Carlos M. Villa
The Dow Chemical Company, Freeport, TX 77541

John M. Wassick
The Dow Chemical Company, Midland, MI 48674

DOI 10.1002/aic.14144
Published online June 6, 2013 in Wiley Online Library (wileyonlinelibrary.com)

The reactor modeling and recipe optimization of conventional semibatch polyether polyol processes, in particular for the polymerization of propylene oxide to make polypropylene glycol, is addressed. A rigorous mathematical reactor model is first developed to describe the dynamic behavior of the polymerization process based on first-principles including the mass and population balances, reaction kinetics, and vapor-liquid equilibria. Next, the obtained differential algebraic model is reformulated by applying a nullspace projection method that results in an equivalent dynamic system with better computational performance. The reactor model is validated against plant data by adjusting model parameters. A dynamic optimization problem is then formulated to optimize the process recipe, where the batch processing time is minimized, given a target product molecular weight as well as other requirements on product quality and process safety. The dynamic optimization problem is translated into a nonlinear program using the simultaneous collocation strategy and further solved with the interior point method to obtain the optimal control profiles. The case study result shows a good match between the model prediction and real plant data, and the optimization approach is able to significantly reduce the batch time by 47%, which indicates great potential for industrial applications. © 2013 American Institute of Chemical Engineers *AIChE J*, 59: 2515–2529, 2013
Keywords: optimization, polymer processing, process control, mathematical modeling

Introduction

Polyether polyols serve as important raw materials in the urethane industry, which represents roughly 5% of the worldwide polymer consumption.[1] Around 90% of all flexible foams produced today are made from polyether type polyols.[2] Other important applications of polyether polyols include polyglycols and surfactants. Similar to other commodity polymers, product quality is measured in many aspects and quantified in indices such as molecular weight (MW) and polydispersity index (PDI). Commercial alkoxylation processes are usually conducted through the reaction of alkylene oxides (e.g. ethylene oxide and/or propylene oxide (PO)) with starters (a.k.a. initiators) containing active hydrogen atoms (e.g. alcohols, amines, or even water). In practice, the polymerization process is catalyzed by a basic catalyst such as potassium hydroxide (KOH) at temperatures above 100°C. A typical example is the anionic polymerization reaction of PO, the modeling of which has been extensively studied from both academic and industrial[2] perspectives. Guibert et al.[3] and Di Serio et al.[4] studied the kinetics of propoxylation processes catalyzed by KOH. In the latter, a kinetic model addressing the initiation, propagation, and cation-exchange reactions was developed as well as vapor-liquid equilibrium (VLE) relations based on modified Raoult's law and Wilson equations. However, both works have not considered the effect of the proton-transfer reaction, which gives rise to a small amount of unsaturated (unsat) monofunctional polymer chains with allyl and propenyl end groups. This reaction leads to impurity in the product polyols that is detrimental for further synthesis of polyurethanes. The transfer reaction was investigated in 1960[5] and more recently by Yu et al.[6] Their research shows that the transfer reaction is typically two orders of magnitude slower than the propagation reaction and is suppressed by hydrogen bonding of hydroxyl groups to active ion pairs. From the industrial point of view, Wegener et al.[7] discussed the use of alternative catalyst systems to reduce the concentration of unsaturated chains and proposed a formula for estimating the actual functionality of polyether polyols taking into account the catalyst type. In addition, Di Serio et al.[8] compared different reactor types commonly adopted in industry for ethoxylation and/or propoxylation and the key factors examined included productivity, energy efficiency, and safety.

Correspondence concerning this article should be addressed to L. T. Biegler at biegler@cmu.edu.

Although widely practiced in experimental research and industrial manufacturing, a comprehensive dynamic reactor model of the propoxylation process, especially with accurate quantitative description of the unsat chain population, is desired for process analysis and technology improvement. Consequently, we first develop a comprehensive first-principles process model in terms of conservation laws, reaction kinetics, and phase equilibria, which results in a system of ordinary differential and algebraic equations (DAEs). Using the developed model, mathematical programming techniques can be conveniently carried over to optimize the process performance. However, detailed modeling of polymerization processes generally leads to large-scale models, for which the computational issue should be carefully addressed, particularly for the sake of optimization. Owing to the advance of dynamic optimization techniques, many successful applications have been reported to improve various polymer product categories, for example, low-density polyethylene,[9] high-impact polystyrene,[10] gas-phase polyolefin,[11,12], polyurethane,[13] and seeded suspension styrene polymerization.[14] The underlying principle of these research studies is to use mechanistic models based on first-principles to predict the dynamic behavior of the process and optimize the process performance by adjusting process control decisions guided by solving associated dynamic optimization problems.

Solution methods of dynamic optimization problems are generally separated into two types, known as the *sequential*[15,16] and *simultaneous*[17] approaches depending on whether the embedded dynamic system is integrated *explicitly* or *implicitly*. In our work, we are particularly interested in the so-called *direct transcription* method (also termed as *the simultaneous collocation method*), a simultaneous approach which is advantageous with respect to numerical stability and constraint handling. The *direct transcription* method avoids explicit integration of state profiles, where a DAE system is fully discretized (both states and controls) using the collocation method[18] over finite elements. By this means, a dynamic optimization problem can be transformed into a large-scale nonlinear program (NLP), featuring favorable sparsity that can be efficiently exploited by existing NLP algorithms.

This article is organized as follows: the next section sets out the development of the reactor model, where the original model is built on first-principles and then a reformulation procedure is carried out to improve the computational efficiency of the model, based on a nullspace projection method. Recipe Optimization Formulation section discusses the dynamic optimization formulation of the recipe improvement problem, addressing the important process constraints. Last, we present a case study, where the model is first validated using plant data and then the optimization results are obtained.

Reactor Model Development

The propoxylation process is a semibatch process that can be carried out in a conventional stirred-tank reactor equipped with heat exchangers for heating and cooling. The starter is formed by mixing the alcohol and catalyst in an appropriate ratio; in certain applications, water is also added which causes hydrolysis of alkylene oxides to form additional alcohols. After the starter is generated, the monomer is fed into the reactor continuously to grow polymers. External heat is required in the start-up stage and soon after the polymerization reactions have been kicked off, a significant amount of heat is released from the reactions and needs to be removed from the tank.

Reaction mechanism

During the anionic polymerization process, each polymer chain undertakes the initiation, propagation, and cation-exchange and proton-transfer reactions. A chain is started when an alkaline anion first reacts with PO, and then the resulting oxy-propylene anion can undertake propagation steps by successively adding monomers through the propagation reaction. The reactivities of chains are affected by the functional end groups; that is, chains ended by hydroxyl groups become dormant while chains with potassium ion can preserve high activity. During polymerization, exchanges of the end groups between species are observed and it is well-known that these reversible reactions are very fast, such that the equilibrium does not influence the polymerization beyond ensuring that all hydroxyl groups in the system serve as equivalent sites of propagation.[6] Last, unsaturated byproducts are formed due to the tendency for rearrangement of PO to allyl alcohol. The process can be classified as a living polymerization system, since the transfer reaction does not terminate chain growth and each chain retains the ability to undertake infinite propagation owing to the presence of the exchange reactions. However, it is worthwhile to note that the transfer reaction creates new chains that live for different but shorter periods than the initial ones.

The following notation is used in the remainder of the article. Let M denote the monomer PO. Let P_n denote the chain $CH_3(PO)_n$, which comprises one of the branches of a polymeric alcohol and n indicates the number of the repeating unit. Meanwhile, U_n represents the unsat chains with double-bond end groups $CH_2{=}CHCH_2(PO)_n$. In addition, W is introduced to account for the presence of water in the initial charge. Furthermore, depending on the different functional end groups, we define

G_n	to denote the growing product chains of length n ($P_nO^-K^+$)
D_n	to denote the dormant product chains of length n (P_nOH)
Q_n	to denote the growing unsat chains of length n ($U_nO^-K^+$)
R_n	to denote the dormant unsat chains of length n (U_nOH)

The reaction schemes can be, therefore, summarized in Table 1. In this work, the kinetic parameters for the product and unsat chains are assumed to be identical for all

Table 1. Reactions in Anionic PO Polymerization

Hydrolysis
$W+M \xrightarrow{k_h} 2D_0$
Initiation
$G_0+M \xrightarrow{k_i} G_1$
$Q_0+M \xrightarrow{k_i} Q_1$
Propagation
$G_n+M \xrightarrow{k_p} G_{n+1}(n \geq 1)$
$Q_n+M \xrightarrow{k_p} Q_{n+1}(n \geq 1)$
Transfer
$G_n+M \xrightarrow{k_t} D_n+Q_0(n \geq 0)$
$Q_n+M \xrightarrow{k_t} R_n+Q_0(n \geq 0)$
Exchange
$G_n+D_m \xrightarrow{k_e} D_n+G_m(n,m \geq 0)$
$Q_n+R_m \xrightarrow{k_e} R_n+Q_m(m,m \geq 0)$
$G_n+R_m \underset{k_e}{\leftrightarrow} D_n+Q_m(n,m \geq 0)$

reactions. Moreover, the asymmetric characteristic of the PO molecule may produce both primary and secondary alcohols in the initiation step, but the latter are found to be dominant.[19] Next in the propagation reaction, the ring-opening insertion of PO can be conducted by either head-to-head, head-to-tail, or tail-to-tail additions (here *head* refers to $CH(CH_3)$ group and *tail* refers to CH_2 group). It is also shown by Heatley et al.[20] that the head-to-tail placement prevails and its proportion is normally above 90%. In this study, the minor reactions stated above are ignored for simplicity. For the transfer reaction, note that the isomerization of allyl end groups to propenyl end groups is not discussed in this work. Finally, the acid-base proton-exchange reactions take place within and across the major and minor populations, and these reactions are reversible and approach equilibrium states. They are the fastest reactions in anionic alkoxylation, and their equilibrium constants are around unity since the acidity of the participating species is similar.[21] Furthermore, the exchange reaction between G and D is expressed with a single reaction rate, because the reactants and products are symmetric, which also applies for Q and R. However, the cross-population-exchange reaction needs two rates to describe it.

First-principles model

The first-principles model consists of population balance equations of polymer chains and monomers, overall mass balances and liquid density correlations, as well as VLE equations. Reactor temperature and monomer feed rate are time-dependent operating decisions, rendering degrees of freedom for process recipe design. According to the reaction schemes described earlier, the population balance equations for individual species can be established as follows

$$\frac{d(V[\mathrm{W}])}{dt} = -Vk_\mathrm{h}[\mathrm{W}][\mathrm{M}] \tag{1a}$$

$$\frac{d(V[\mathrm{G}_0])}{dt} = -Vk_\mathrm{i}[\mathrm{G}_0][\mathrm{M}] - Vk_\mathrm{t}[\mathrm{G}_0][\mathrm{M}] - Vk_\mathrm{e}[\mathrm{G}_0]\sum_{m=0}^{N}([\mathrm{D}_m] + [\mathrm{R}_m]) + Vk_\mathrm{e}[\mathrm{D}_0]\sum_{m=0}^{N}([\mathrm{G}_m] + [\mathrm{Q}_m]) \tag{1b}$$

$$\frac{d(V[\mathrm{G}_1])}{dt} = V\left(k_\mathrm{i}[\mathrm{G}_0] - k_\mathrm{p}[\mathrm{G}_1]\right)[\mathrm{M}] - Vk_\mathrm{t}[\mathrm{G}_1][\mathrm{M}] - Vk_\mathrm{e}[\mathrm{G}_1]\sum_{m=0}^{N}([\mathrm{D}_m] + [\mathrm{R}_m]) + Vk_\mathrm{e}[\mathrm{D}_1]\sum_{m=0}^{N}([\mathrm{G}_m] + [\mathrm{Q}_m]) \tag{1c}$$

$$\frac{d(V[\mathrm{G}_n])}{dt} = Vk_\mathrm{p}([\mathrm{G}_{n-1}] - [\mathrm{G}_n])[\mathrm{M}] - Vk_\mathrm{t}[\mathrm{G}_n][\mathrm{M}] - Vk_\mathrm{e}[\mathrm{G}_n]\sum_{m=0}^{N}([\mathrm{D}_m] + [\mathrm{R}_m]) + Vk_\mathrm{e}[\mathrm{D}_n]\sum_{m=0}^{N}([\mathrm{G}_m] + [\mathrm{Q}_m]), \quad n = 2, \ldots, N-1 \tag{1d}$$

$$\frac{d(V[\mathrm{G}_N])}{dt} = Vk_\mathrm{p}([\mathrm{G}_{N-1}])[\mathrm{M}] - Vk_\mathrm{t}[\mathrm{G}_N][\mathrm{M}] - Vk_\mathrm{e}[\mathrm{G}_N]\sum_{m=0}^{N}([\mathrm{D}_m] + [\mathrm{R}_m]) + Vk_\mathrm{e}[\mathrm{D}_N]\sum_{m=0}^{N}([\mathrm{G}_m] + [\mathrm{Q}_m]) \tag{1e}$$

$$\frac{d(V[\mathrm{D}_0])}{dt} = V2k_\mathrm{h}[\mathrm{W}][\mathrm{M}] + Vk_\mathrm{t}[\mathrm{G}_0][\mathrm{M}] + Vk_\mathrm{e}[\mathrm{G}_0]\sum_{m=0}^{N}([\mathrm{D}_m] + [\mathrm{R}_m]) - Vk_\mathrm{e}[\mathrm{D}_0]\sum_{m=0}^{N}([\mathrm{G}_m] + [\mathrm{Q}_m]) \tag{1f}$$

$$\frac{d(V[\mathrm{D}_n])}{dt} = Vk_\mathrm{t}[\mathrm{G}_n][\mathrm{M}] + Vk_\mathrm{e}[\mathrm{G}_n]\sum_{m=0}^{N}([\mathrm{D}_m] + [\mathrm{R}_m]) - Vk_\mathrm{e}[\mathrm{D}_n]\sum_{m=0}^{N}([\mathrm{G}_m] + [\mathrm{Q}_m]), \quad n = 1, \ldots, N \tag{1g}$$

$$\frac{d(V[\mathrm{Q}_0])}{dt} = -Vk_\mathrm{i}[\mathrm{Q}_0][\mathrm{M}] + Vk_\mathrm{t}\sum_{n=0}^{N}([\mathrm{G}_n] + [\mathrm{Q}_n])[\mathrm{M}] - Vk_\mathrm{t}[\mathrm{Q}_0][\mathrm{M}] - Vk_\mathrm{e}[\mathrm{Q}_0]\sum_{m=0}^{N}([\mathrm{D}_m] + [\mathrm{R}_m]) + Vk_\mathrm{e}[\mathrm{R}_0]\sum_{m=0}^{N}([\mathrm{G}_m] + [\mathrm{Q}_m]) \tag{1h}$$

$$\frac{d(V[\mathrm{Q}_1])}{dt} = V\left(k_\mathrm{i}[\mathrm{Q}_0] - k_\mathrm{p}[\mathrm{Q}_1]\right)[\mathrm{M}] - Vk_\mathrm{t}[\mathrm{Q}_1][\mathrm{M}] - Vk_\mathrm{e}[\mathrm{Q}_1]\sum_{m=0}^{N}([\mathrm{D}_m] + [\mathrm{R}_m]) + Vk_\mathrm{e}[\mathrm{R}_1]\sum_{m=0}^{N}([\mathrm{G}_m] + [\mathrm{Q}_m]) \tag{1i}$$

$$\frac{d(V[\mathrm{Q}_n])}{dt} = Vk_\mathrm{p}([\mathrm{Q}_{n-1}] - [\mathrm{Q}_n])[\mathrm{M}] - Vk_\mathrm{t}[\mathrm{Q}_n][\mathrm{M}] - Vk_\mathrm{e}[\mathrm{Q}_n]\sum_{m=0}^{N}([\mathrm{D}_m] + [\mathrm{R}_m]) + Vk_\mathrm{e}[\mathrm{R}_n]\sum_{m=0}^{N}([\mathrm{G}_m] + [\mathrm{Q}_m]), \quad n = 2, \ldots, N-1 \tag{1j}$$

$$\frac{d(V[\mathrm{Q}_N])}{dt} = Vk_\mathrm{p}([\mathrm{Q}_{N-1}])[\mathrm{M}] - Vk_\mathrm{t}[\mathrm{Q}_N][\mathrm{M}] - Vk_\mathrm{e}[\mathrm{Q}_N]\sum_{m=0}^{N}([\mathrm{D}_m] + [\mathrm{R}_m]) + Vk_\mathrm{e}[\mathrm{R}_N]\sum_{m=0}^{N}([\mathrm{G}_m] + [\mathrm{Q}_m]) \tag{1k}$$

$$\frac{d(V[\mathrm{R}_n])}{dt} = Vk_\mathrm{t}[\mathrm{Q}_n][\mathrm{M}] + Vk_\mathrm{e}[\mathrm{Q}_n]\sum_{m=0}^{N}([\mathrm{D}_m] + [\mathrm{R}_m]) - Vk_\mathrm{e}[\mathrm{R}_n]\sum_{m=0}^{N}([\mathrm{G}_m] + [\mathrm{Q}_m]), \quad n = 0, 1, \ldots, N \tag{1l}$$

Here, V is the volume of the liquid in the reactor and $[\cdot]$ denotes the liquid-phase concentration. Moreover, to make computation tractable, a sufficiently large number N is chosen to denote the length of the longest chains that are recorded in the model and chains beyond N are ignored. In addition, chains with N repeating units are assumed not to undertake propagation reactions. Commercial polyether type polyols typically have chain lengths less than 100[22] so that the resultant model sizes remain manageable even when the detailed population spectrum is calculated. For the monomer balance, the external feed is entering the reactor at rate F,

and the monomers are consumed by all four reactions (hydrolysis, initiation, propagation, and transfer)

$$\frac{d(V[\mathrm{M}])}{dt}=F-V\left(k_{\mathrm{h}}[\mathrm{W}]+k_{\mathrm{i}}([\mathrm{G}_0]+[\mathrm{Q}_0])+k_{\mathrm{p}}\sum_{n=1}^{N-1}([\mathrm{G}_n]+[\mathrm{Q}_n])+k_{\mathrm{t}}\sum_{n=0}^{N}([\mathrm{G}_n]+[\mathrm{Q}_n])\right)[\mathrm{M}] \tag{2}$$

For the total mass balance, as the monomer enters the system, we have

$$\frac{dm}{dt}=F\mathrm{MW}_{\mathrm{PO}} \tag{3}$$

where $\mathrm{MW}_{\mathrm{PO}}$ denotes the MW of PO and m is the total mass of the polymerization system. The liquid density is solely dependent on the reactor temperature since the effects of MW on density are found to be minor. Therefore, the liquid volume is calculated by[23]

$$V=m\left(10^{-6}+7.576\times10^{-10}(T-298.15)\right) \tag{4}$$

Although the polymerization reactions occur only in the liquid phase, a faithful VLE model is still important for the purpose of process monitoring in manufacturing practice. Reactor pressure measures are often convenient to obtain and can be used to infer the unreacted PO concentration in the liquid, which is difficult and also risky to measure directly. For a dummy volatile component i, the basic equation of the vapor-liquid-phase equilibrium is written as

$$P_{\mathrm{i}}=a_{\mathrm{i}}P_{\mathrm{i}}^{\mathrm{sat}} \tag{5}$$

where P_{i}, a_{i}, and $P_{\mathrm{i}}^{\mathrm{sat}}$ are the partial pressure, liquid-phase activity, and saturated vapor pressure of component i, respectively. The total pressure of the reactor P can be obtained by

$$P=\sum_{\mathrm{i}}P_{\mathrm{i}} \tag{6}$$

Typically, PO is considered to be volatile, and other possible volatile components include water and starters. However, PO polyols are liquids in the MW range of 200–6000[23]. It follows the assumption that no polymers exist in the vapor-phase. In addition, Eq. 6 may be adjusted in the presence of nitrogen in the reactor by also including the partial pressure over this nonvolatile component. The vapor pressure can be calculated using the Antoine equation

$$\log_{10}P_{\mathrm{i}}^{\mathrm{sat}}=A_{\mathrm{i}}-\frac{B_{\mathrm{i}}}{T+C_{\mathrm{i}}} \tag{7}$$

For the polymer-solvent equilibrium, the Flory-Huggins theory[24] provides a rational method to develop an expression for the activity of a solvent in a polymer. In this study, the liquid mixture contains multicomponent solvents that complicates the calculation. A simple yet effective approximation is to treat the system as a pseudo binary mixture, where the solvent is PO (denoted in index s) and the other components are assumed to be the polymer (denoted in index p). The simplification is reasonable since by the time polyols are present in sufficient amounts to dominate VLE, both initiator and water have been almost fully reacted. Hence, the activity of PO is equal to

$$\ln a_{\mathrm{s}}=\ln\phi_{\mathrm{s}}+\left(1-\frac{1}{l}\right)\phi_{\mathrm{p}}+\chi\phi_{\mathrm{p}}^2 \tag{8}$$

In Eq. 8, rather than using mole fractions, the fractions of lattice sites occupied by the solvent molecule ϕ_{s} and polymer ϕ_{p} are applied. The interaction parameter χ is nondimensional and accounts for the energy of interdispersing polymer and solvent molecules. While polyols are small polymers compared to many other commercial ones, the effect of the number-average chain length l still needs to be taken into account when calculating the lattice fraction, shown as below

$$\phi_{\mathrm{s}}=\frac{n_{\mathrm{s}}}{n_{\mathrm{s}}+n_{\mathrm{p}}l} \tag{9a}$$

$$\phi_{\mathrm{p}}=\frac{n_{\mathrm{p}}l}{n_{\mathrm{s}}+n_{\mathrm{p}}l} \tag{9b}$$

Here, n_{s} and n_{p} represent the numbers of molecules of the solvent (PO) and the polymer, respectively, calculated as

$$n_{\mathrm{s}}=V[\mathrm{M}] \tag{10a}$$

$$n_{\mathrm{p}}=V\left([\mathrm{W}]+\sum_{n=0}^{N}([\mathrm{G}_n]+[\mathrm{D}_n]+[\mathrm{Q}_n]+[\mathrm{R}_n])\right) \tag{10b}$$

Conversely, the activities of other volatile components such as water can be treated as constants for simplicity. To this end, the first-principles reactor model for describing the propoxylation process is complete. This model comprises DAEs, and the involved differential and algebraic state variables can reveal detailed information of the system. The population distribution for all species is recoded in a chain length basis over the operation time horizon.

Reformulation of the exchange reactions

Synergistic fast and slow dynamic modes are often encountered in modeling chemical dynamic systems and cause difficulties in their numerical solution. Therefore, a reformulation procedure is required but it is often nontrivial to obtain by intuition, giving correct asymptotic characteristics. The reformulation and model reduction of such systems have been investigated by Daoutidis and coworkers, particularly in the context of solvent recycles.[25] The underlying idea is to separate the fast and the slow components in a DAE system by describing the fast ones with algebraic equations capturing their quasi-steady states. As a result, the reformulated system becomes less stiff but with the same asymptotic behavior. As noted earlier, among the polymerization reactions, the rates of the exchange reactions are significantly higher than those of the other reactions. Modeling the polymerization system consequently leads to a two-time-scale model and incurs the stiffness issue of the resulting DAE model derived in Eqs. 1a–11. To address this challenge, a nullspace projection method is discussed in the sequel, following a similar idea as the aforementioned one.

Nullspace projection. We develop a systematic reformulation procedure of reaction equation systems that is based

on a nullspace projection method. Here, we consider a general reaction system given by

$$\dot{x} = Ar(x) + g(t) \tag{10}$$

where $x \in \mathbb{R}^{n_x}$ is the vector of component concentrations/populations, $r(x) \in \mathbb{R}^{n_r}$ is the vector of reaction rates, $A \in \mathbb{R}^{n_x} \times \mathbb{R}^{n_r}$ is the coefficient matrix, and $g(t) \in \mathbb{R}^{n_x}$ represents the external input such that $g(t) \not\equiv 0$ for fed-batch reactions and $g(t) \equiv 0$ for batch reactions. For the reactions, we partition $r(x)$ so that reactions that reach equilibrium are separated from those that do not, and the coefficients in matrix A are partitioned accordingly, written as

$$\dot{x} = [A_1 \quad A_2] \begin{bmatrix} r_1(x) \\ \sigma r_2(x) \end{bmatrix} + g(t) \tag{11}$$

In the equation, $\sigma r_2(x)$ represents the rates of equilibrium reactions, where σ is a large positive number that can approach infinity. Next, a nullspace matrix $\mathcal{Z}$ is introduced such that $\mathcal{Z}^{\mathrm{T}} A_2 = 0$, and a corresponding matrix $\mathcal{Y}$ spanning the range space of A_2 is also defined, ensuring $[\mathcal{Y} \quad \mathcal{Z}] \in \mathbb{R}^{n_x} \times \mathbb{R}^{n_x}$ is nonsingular. Multiplying the transposed matrix $[\mathcal{Y} \quad \mathcal{Z}]^{\mathrm{T}}$ to the two sides of Eq. 25, it gives

$$\mathcal{Y}^{\mathrm{T}} \dot{x} = \mathcal{Y}^{\mathrm{T}} A_1 r_1(x) + \sigma \mathcal{Y}^{\mathrm{T}} A_2 r_2(x) + \mathcal{Y}^{\mathrm{T}} g(t) \tag{13a}$$

$$\mathcal{Z}^{\mathrm{T}} \dot{x} = \mathcal{Z}^{\mathrm{T}} A_1 r_1(x) + \mathcal{Z}^{\mathrm{T}} g(t) \tag{13b}$$

Equation 13b does not include equilibrium rates, and it is kept as a part of the reformulated system. Conversely, the matrices in Eq. 13a can be further rearranged and partitioned; on the right-hand side, $\sigma \mathcal{Y}^{\mathrm{T}} A_2 r_2(x)$ corresponds to the effect of equilibrium rates and it can be separated into a zero and a non-zero part; and $\mathcal{Y}$ can be partitioned accordingly. Let $f(x)$ denote the non-zero elements in $\mathcal{Y}^{\mathrm{T}} A_2 r_2(x)$, and partitioning these elements leads to

$$\begin{bmatrix} \mathcal{Y}_a{}^{\mathrm{T}} \\ \mathcal{Y}_b{}^{\mathrm{T}} \end{bmatrix} \dot{x} = \begin{bmatrix} \mathcal{Y}_a{}^{\mathrm{T}} \\ \mathcal{Y}_b{}^{\mathrm{T}} \end{bmatrix} A_1 r_1(x) + \begin{bmatrix} 0 \\ \sigma f(x) \end{bmatrix} + \begin{bmatrix} \mathcal{Y}_a{}^{\mathrm{T}} \\ \mathcal{Y}_b{}^{\mathrm{T}} \end{bmatrix} g(t) \tag{14}$$

When $\sigma \to \infty$, the rows corresponding to zeros in the second term on the right-hand side (zero rows in $\sigma \mathcal{Y}^{\mathrm{T}} A_2 r_2(x)$) remain unaffected and $f(x) = 0$ is required for the rest of the rows in the equation. In fact, $f(x) = 0$ sketches the equilibrium manifold of the fast reaction system, as a quasi-steady-state solution that should be included in the reformulated system. In sum, the reformulated DAE system is shown as below

$$\mathcal{Y}_a{}^{\mathrm{T}} \dot{x} = \mathcal{Y}_a{}^{\mathrm{T}} A_1 r_1(x) + \mathcal{Y}_a{}^{\mathrm{T}} g(t) \tag{15a}$$

$$f(x) = 0 \tag{15b}$$

$$\mathcal{Z}^{\mathrm{T}} \dot{x} = \mathcal{Z}^{\mathrm{T}} A_1 r_1(x) + \mathcal{Z}^{\mathrm{T}} g(t) \tag{15c}$$

Reformulated propoxylation reactor model. Applying the nullspace projection method, the reformulated model can be derived after a sequence of matrix operations. For detailed information, please refer to Appendix A. As a result of the reformulation procedure, two pseudospecies X and Y are introduced

$$\begin{aligned} \mathrm{X}_n &= \mathrm{G}_n + \mathrm{D}_n, \qquad n = 0, 1, \ldots, N \\ \mathrm{Y}_n &= \mathrm{Q}_n + \mathrm{R}_n, \qquad n = 0, 1, \ldots, N \end{aligned} \tag{16}$$

In fact, X refers to the polyol product and Y the unsaturated byproduct. Following the reformulated system shown in Eqs. 15a–15c, the nullspace multiplication (Eq. 15c) leads to a group of population balances that are not affected by the exchange reactions, which can be written in the form of concentrations:

$$\frac{d(V[\mathrm{X}_0])}{dt} = V(2k_{\mathrm{h}}[\mathrm{W}] - k_{\mathrm{i}}[\mathrm{G}_0])[\mathrm{M}] \tag{17a}$$

$$\frac{d(V[\mathrm{X}_1])}{dt} = V\left(k_{\mathrm{i}}[\mathrm{G}_0] - k_{\mathrm{p}}[\mathrm{G}_1]\right)[\mathrm{M}] \tag{17b}$$

$$\frac{d(V[\mathrm{X}_n])}{dt} = Vk_{\mathrm{p}}([\mathrm{G}_{n-1}] - [\mathrm{G}_n])[\mathrm{M}], \qquad n = 2, \ldots, N-1 \tag{17c}$$

$$\frac{d(V[\mathrm{X}_N])}{dt} = Vk_{\mathrm{p}}[\mathrm{G}_{N-1}][\mathrm{M}] \tag{17d}$$

$$\frac{d(V[\mathrm{Y}_0])}{dt} = -Vk_{\mathrm{i}}[\mathrm{Q}_0][\mathrm{M}] + Vk_{\mathrm{t}} \sum_{n=0}^{N} ([\mathrm{G}_n] + [\mathrm{Q}_n])[\mathrm{M}] \tag{17e}$$

$$\frac{d(V[\mathrm{Y}_1])}{dt} = V\left(k_{\mathrm{i}}[\mathrm{Q}_0] - k_{\mathrm{p}}[\mathrm{Q}_1]\right)[\mathrm{M}] \tag{17f}$$

$$\frac{d(V[\mathrm{Y}_n])}{dt} = Vk_{\mathrm{p}}([\mathrm{Q}_{n-1}] - [\mathrm{Q}_n])[\mathrm{M}], \qquad n = 2, \ldots, N-1 \tag{17g}$$

$$\frac{d(V[\mathrm{Y}_N])}{dt} = Vk_{\mathrm{p}}[\mathrm{Q}_{N-1}][\mathrm{M}] \tag{17h}$$

In Eq. 13a, the range space term $\mathcal{Y}^{\mathrm{T}} A_2$ has two zero rows, corresponding to the balance equations of the water and monomer, and Eq. 15a renders the same equations as stated in Eqs. 1a and 2. The quasi-steady-state manifolds are obtained using Eq. 15b

$$[\mathrm{G}_n] \sum_{m=0}^{N} ([\mathrm{D}_m] + [\mathrm{R}_m]) = [\mathrm{D}_n] \sum_{m=0}^{N} ([\mathrm{G}_m] + [\mathrm{Q}_m]), \qquad n = 0, 1, \ldots, N \tag{18a}$$

$$[\mathrm{Q}_n] \sum_{m=0}^{N} ([\mathrm{D}_m] + [\mathrm{R}_m]) = [\mathrm{R}_n] \sum_{m=0}^{N} ([\mathrm{G}_m] + [\mathrm{Q}_m]), \qquad n = 0, 1, \ldots, N \tag{18b}$$

To this end, the reformulation procedure is complete with Eqs. 16−18. Furthermore, the total amount of catalyst is equal to the amount of chains with K^+ ions, denoted as

$$n_{\mathrm{c}} = V \sum_{n=0}^{N} ([\mathrm{G}_n] + [\mathrm{Q}_n]) \tag{19}$$

and additionally, we introduce n_{i} as the total number of moles of the initiator

$$n_{\mathrm{i}} = V \sum_{n=0}^{N} ([\mathrm{G}_n] + [\mathrm{D}_n]) \tag{20}$$

and the total moles of the unsaturated chains

$$n_{\mathrm{u}} = V \sum_{n=0}^{N} ([\mathrm{Q}_n] + [\mathrm{R}_n]) \tag{21}$$

As a result, Eqs. 16 and 18 can be further reduced to

$$\begin{aligned} \mathrm{X}_n n_{\mathrm{c}} &= \mathrm{G}_n (n_{\mathrm{i}} + n_{\mathrm{u}}), \qquad n = 0, 1, \ldots, N \\ \mathrm{Y}_n n_{\mathrm{c}} &= \mathrm{Q}_n (n_{\mathrm{i}} + n_{\mathrm{u}}), \qquad n = 0, 1, \ldots, N \end{aligned} \tag{22}$$

Using the definition of n_{c}, the right-hand side of Eq. 17e can also be simplified because n_{c} is constant for most applications. In sum, the reformulated model consists of

Population balances	Eq. 17
Quasi-steady states	Eq. 22 and definitions in Eqs. 19−21
Additional equations	Monomer balance (Eq. 2) Volume determination (Eqs. 3 and 4) VLE relations (Eqs. 5−9)

Note that although the original stiff differential systems can be numerically handled by the Gear type methods, the nullspace projection procedure is a better solution. It gives an open equation system for optimization purposes. Also, the reformulated model is superior to the earlier one because it eliminates the fast dynamic modes in the differential equations, such that the DAE system becomes less stiff with a reduced number of differential equations.

Recipe Optimization Formulation

The recipe for a batch/semibatch operation is often designed *off-line* based on the experience of past production runs. For many industrial processes, process recipe improvement is only carried out manually based on laboratory experiments and process simulation programs. However, given the dynamic model developed above, more rigorous model-based optimization methods can be exploited, providing more insight of the process and accurate calculation results. In this study, the optimization problem is formulated to minimize the batch time by designing the optimum reactor temperature and monomer feeding profiles. The constraints on the process deal with the final product quality and process safety regulations, including the target product MW as well as thresholds on byproduct formation, unreacted monomer, reactor temperature, etc.

Product quality and process safety constraints

In the polyol industry, a number of quantities have been widely used to characterize the product performance, such as the MW, level of unsaturated monofunctional chains (termed as unsat number in the remainder), functionality, hydroxyl number, and PDI. These indices are greatly influenced by the choice of the starting alcohol and initial charge condition and are also subject to the variation of operating conditions. All these quality indices can be readily calculated given the type of the starter used and the population distribution of the polyol. In this work, we consider the target number-average MW and unsat number as key quality requirements that the optimized recipe should satisfy. To calculate the number-average MW, we introduce the notation of polymer moments. By definition, the kth moment of a polymer species (e.g. X) is written as

$$\gamma_k = \sum_{n=1}^{N} n^k \mathrm{X}_n, \qquad k = 0, 1, \ldots \tag{23}$$

and the number-average MW can then be defined further as the ratio of the first and zeroth moment, multiplied by the MW of the repeating unit

$$M_n = \mathrm{MW}_{\mathrm{PO}} \frac{\gamma_1}{\gamma_0} \tag{24}$$

Note that the ratio of the first and zeroth moment also represents the number-average chain length of the polymer. Similarly, for the weight-average molecular weight M_w, we define

$$M_w = \mathrm{MW}_{\mathrm{PO}} \frac{\gamma_2}{\gamma_1} \tag{25}$$

Moreover, the ratio of the M_w over M_n defines PDI, which is an index that accounts for the spread of the molecular distribution

$$\mathrm{PDI} = \frac{M_w}{M_n} \tag{26}$$

The unsat number calibrates the concentration of monofunctional chains in the final product. It is defined as the milliequivalents of unsat chains per total mass

$$\mathrm{unsat} = 1000 \frac{n_{\mathrm{u}}}{m} \tag{27}$$

The monofunctionality is undesired because it generally decreases the functionality that in consequence strongly affects the viscosity of the product; thus, corresponding upper bounds should be enforced with regard to specific product categories and applications. Also, the concentration of unreacted monomer in the final polyol product should be maintained under proper limits. Conventionally, it is measured in parts per million (ppm), as shown below

$$\mathrm{unrct} = \mathrm{MW}_{\mathrm{PO}} \frac{\mathrm{M}}{m} \times 10^6 \tag{28}$$

Functionality is defined as the ratio of the total amount of hydroxyl groups from the initiator and monol over the total amount of all types of polymer chains

$$f = \frac{N_{\mathrm{OH}} n_{\mathrm{i}} + n_{\mathrm{u}}}{n_{\mathrm{i}} + n_{\mathrm{u}}} \tag{29}$$

In the definition, N_{OH} corresponds to the number of branches of the initial alcohol molecule ($N_{\mathrm{OH}} = 2$ for propylene glycol (PG)). And also, the hydroxyl equivalent weight (HEW) is defined as the number-average MW divided by the functionality

$$\mathrm{HEW} = \frac{M_n}{f} \tag{30}$$

Last, the number of hydroxyl groups (OH#) gives the hydroxyl content of a polyol, calculated by using the equivalent weight of KOH

$$\mathrm{OH\#} = \frac{1000 \mathrm{MW}_{\mathrm{KOH}}}{\mathrm{HEW}} \tag{31}$$

Conversely, process safety is always a vital concern in the polymerization reaction process. To derive the safety constraints, we first write a simplified energy balance equation of the reactor by only considering the propagation reaction as the source of reaction heat

$$\frac{d(mH_{\mathrm{b}})}{dt} = F \Delta H_{\mathrm{f}} \mathrm{MW}_{\mathrm{PO}} + r_{\mathrm{p}} \left(-\Delta H_{\mathrm{p}}\right) \mathrm{MW}_{\mathrm{PO}} - q \tag{32}$$

where r_{p} is the lumped rate of all propagation reactions, and the heat of reaction $-\Delta H_{\mathrm{p}}$ is assumed to be constant (see Table B3). Also, q denotes the heat removal rate from the

heat exchanger that can be determined using the overall heat-transfer coefficient U and area A

$$q=UA(T-T_{\mathrm{w}}) \tag{33}$$

where T_{w} is the temperature of the water used by the heat exchanger, and it is assumed to be constant. In Eq. 32, the enthalpies of the feed flow and bulk liquid are H_{f} and H_{b}, respectively, which are defined as

$$H_{\mathrm{i}}=\int c_{p\mathrm{i}}dT, \qquad \mathrm{i}=\{f,b\}. \tag{34}$$

The heat capacity of the feed monomer $c_{p\mathrm{f}}$ is cubic with respect to temperature, and the bulk heat capacity $c_{p\mathrm{b}}$ can be estimated by the heat capacity of the product polyol, which is almost linear with temperature, as noted in Table B1

For the first safety constraint, the heat removal duty cannot exceed the allowed maximum cooling capacity of the heat exchanger attached to the reactor

$$r_{\mathrm{p}}\left(-\Delta H_{\mathrm{p}}\right)\mathrm{MW}_{\mathrm{PO}} \le F(-\Delta H_{\mathrm{f}})\mathrm{MW}_{\mathrm{PO}}+UA(T-T_{\mathrm{w}}) \tag{35}$$

Here, we assume the monomer feed enters at a constant temperature $T_{\mathrm{m}}=25^{\circ}\mathrm{C}$, which is lower than the reactor temperature, offering extra cooling capability in addition to the heat exchanger capacity. The term UA represents the heat-transfer efficiency that is known as a constant. Second, for the polyol process, the amount of unreacted oxides present in the reactor should be carefully controlled to prevent the plant from risks of product decomposition, under the accidental circumstance that the plant losses its cooling capability during operations. To carry out such a task, it is conducive to add a constraint on the *adiabatic end temperature*,[26] which equals the summation of the current reactor temperature and the potential adiabatic temperature rise due to the occurrence of *total loss of cooling*. When the heat exchanger breaks down at time t_{c} with the reactor temperature noted as T_{c}, it is clear that $q=0$ and also reasonable to assume $F=0$ after t_{c}. Therefore, integrating Eq. 32 starting from t_{c} to the steady state (infinity) gives

$$m(H_{\mathrm{b}}(T_{\mathrm{ad}})-H_{\mathrm{b}}(T_{\mathrm{c}}))=V[\mathrm{M}]\mathrm{MW}_{\mathrm{PO}}\left(-\Delta H_{\mathrm{p}}\right) \tag{36}$$

where T_{ad} is the adiabatic end temperature and we assume all the monomers are consumed in the propagation reactions. For the safety limit of the adiabatic end temperature, a sufficient safety margin is also needed to tolerate uncertainties, where a recommended value of 250°C is reported in a patent document.[27]

Dynamic optimization formulation

In the overall formulation, the process recipe is optimized to shorten the operating time demanded for polymerization and the optimization model consists of the reformulated reactor model and additional process constraints; this leads to a large set of DAEs. The problem can be written in a general form as a dynamic optimization problem

$$\min_{u\in \mathrm{U}} t_{\mathrm{f}} \tag{37a}$$

$$\text{s.t.} \quad \begin{aligned} &\dot{z}=f(z(t),y(t),u(t)), \qquad z(0)=z_0\\ &g(z(t),y(t),u(t))=0\\ &h(z(t),y(t),u(t)) \ge 0\\ &t\in[0,t_{\mathrm{f}}] \end{aligned} \tag{37b}$$

Here, z and y are differential and algebraic state variables, respectively, and u denotes the control variables that in this study include the reactor temperature and monomer feeding rate. The reformulated model is represented by the DAEs in $f(\cdot)$ and $g(\cdot)$, while the process constraints are noted by $h(\cdot)$. The constraint $h(\cdot)$ can be enforced either at final time by restricting $t=t_{\mathrm{f}}$ or along the whole path when $t\in[0,t_{\mathrm{f}}]$. In this study, the initial condition of the differential variables z_0 is given by the charge condition of the batch. The total length of the operation equals t_{f}, the objective function to be minimized.

Solution Strategy

As noted earlier, we adopt the simultaneous collocation method to deal with the dynamic optimization problem for optimizing the process recipe. The method follows a full discretization methodology, in which orthogonal collocation on a fixed/moving finite element mesh is introduced to represent the continuous time horizon. The control decisions are usually parametrized within finite elements using piecewise constant or linear profiles. Meanwhile, the state variables are also discretized in the time dimension, and also, the discretization scheme used for the states can be finer than the one used for controls. More specifically, for the differential states, a *Runge-Kutta* basis representation is introduced

$$z(t)=z_{i-1}+h_i\sum_{j=1}^{K}\Omega_j(\tau)\dot{z}_{i,j} \tag{38}$$

where i is the index of finite elements and j corresponds to collocation points up to K; h_i is the length of the element; $\tau\in[0,1]$ is the normalized time in an element with $t=t_{i-1}+h_i\tau$; z_{i-1} is the value of the differential variable at the beginning of the element; $\dot{z}_{i,j}$ is the value of the first derivatives at collocation points; and Ω_j is a polynomial of τ of order K, defined as

$$\Omega_j=\int_0^{\tau}\ell_j(\tau')d\tau' \tag{39}$$

In the definition, ℓ_j is an orthogonal basis function, where Lagrange interpolation polynomials are often used by virtue of their exactness at collocation points, shown as

$$\ell_j(\tau)=\prod_{j'=1,\neq j}^{K}\frac{\tau-\tau_{j'}}{\tau_j-\tau_{j'}} \tag{40}$$

In addition, to ensure the continuity condition across element boundaries, the following equation is introduced

$$z_i=z_{i-1}+h_i\sum_{j=1}^{K}\Omega_j(1)\dot{z}_{i,j} \tag{41}$$

The algebraic states y are treated as K^{th} order Lagrange polynomials, but without the continuity condition across finite elements. To this end, the dynamic optimization problem 37 has been translated into a continuous NLP with a sparse structure, as described by Biegler.[17] A number of NLP solvers are applicable for the problem, for example, the generalized reduced gradient algorithm (CONOPT[28]) and the interior point method (IPOPT[29]).

Case Study

In the case study, the process of interest is the production of a low MW polypropylene glycol (M_n=950g/mol) from the polymerization of PO initiated by water and PG. The product is widely used in applications such as coating and surfactants. For this example, the basic ingredients are given as follows:

Starter	PG and water
Catalyst	KOH
Monomer	PO

Model implementation

The polymerization model is implemented in the General Algebraic Modeling System (GAMS)[30] platform after discretization into an NLP. The size of the model is largely determined by the discretization setting and the number of the recorded chain length limit. A careful choice is required to balance the accuracy and computational load of the model. In this study, we assume the controls are represented by piecewise linear functions that preserve continuity over finite elements, and 24 equidistant finite elements are used along with three Radau collocation points in the orthogonal collocation scheme. The chain length distribution is truncated at $N = 18$, which is large enough to accommodate the long chains.

Initially, we test the fidelity of the developed first-principles model. To validate the model against plant data, the participating model parameters such as kinetic constants and thermodynamic properties need to be adjusted such that the model can adequately represent the real process, despite the imposed assumptions made and process uncertainties. The adjustment actions are based on the understanding and experience with the process, aiming to deal with deficiencies of the original process model.[31] Next, optimization is performed over the verified model, but allowing for variations of the reactor temperature and feed rate in certain ranges.

Model validation

In this study, the reactor pressure profile is used as the main criterion for tuning to illustrate the validation procedure. In fact, a much more detailed validation with polymer quality indices has also been done, but proprietary considerations prevent us from presenting more information here. To obtain the pressure, the VLE calculations from Eqs. 5−9 are essential but further complicated in the presence of nitrogen and a vent system control valve in the reactor.

First, the nitrogen inside the reactor tank contributes to the total pressure. As the polymerization takes place, the nitrogen partial pressure rises over time since the liquid volume expands and compresses the gases. Assume the initial amount of nitrogen n_{N_2} is known, then the real-time partial pressure over N_2 can be obtained by the ideal gas law, since the reactor pressure is not very high

$$P_{N_2}\bar{V} = n_{N_2}RT \tag{42}$$

Here, the gas-phase volume $\bar{V}$ equals the total reactor volume minus the liquid-phase volume V. Note that the total reactor pressure in Eq. 6 also includes the partial pressure of nitrogen. Next, the installed control valve avoids extreme pressures in the reactor tank: once the total pressure exceeds the upper limit P^{max}, the valve opens and keeps the pressure below P^{max}. This operation does not affect the reactions in the liquid phase, if we assume a negligible loss of the vapor-phase PO when the system is vented. In addition, as nitrogen escapes, n_{N_2} decreases in time. The amount of released nitrogen can be estimated using Eq. 42 as the gas-phase volume decreases and the reactor pressure stays constant at the maximum allowed by the vent system. A base recipe from real plant data is used for model calibration, where the batch time is normalized to unity, and the reactor temperature, monomer feeding rate, and pressure are recorded during each sampling interval. For this particular example, we consider the model prediction and real plant pressure profiles under the same operating conditions, and the result is shown in Figure 1 in comparison. The model exhibits satisfactory performance in pressure prediction, and the discrepancy after valve relief is still acceptable, given the simplification made for gas release. The estimated partial pressures are also depicted. Note that for the last 6% of the operation time, the corresponding plant data are not plotted due to full reactor venting. The major parameter adjustments are regarding reaction kinetics: all the kinetic constants are first obtained from published articles; next the pre-exponential factors are tuned to best fit the model predicted pressure to the plant data. Please refer to Appendix B for details.

Recipe optimization results

Optimization is carried out with respect to the same polymerization system, with the following constraints added:

1. The final number-average MW of the polymer is no less than 950 g/mol.

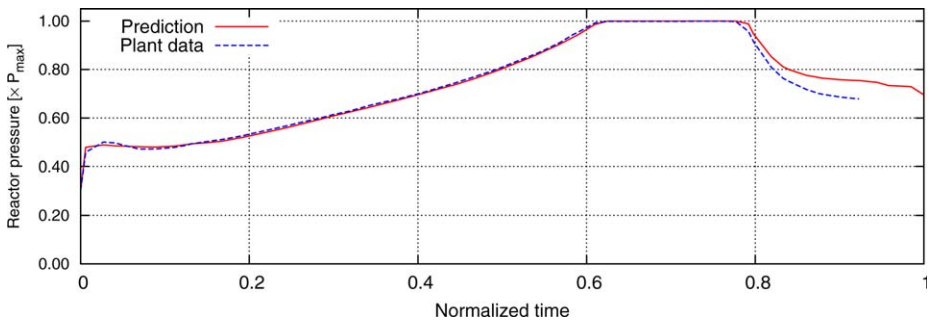

Figure 1. Reactor pressure profiles.

[Color figure can be viewed in the online issue, which is available at wileyonlinelibrary.com.]

Table 2. Recipe Optimization Model Statistics and Results

Opt. Soln	MW (g/mol)	Unsat (mmol/g)	PO (ppm)	# of Var.	# of Con.	CPU (s)
0.53	950	0.033	120	10,946	11,043	56

2. The maximum unsaturation value is 0.033 mmol/g polyol.
3. The final unreacted PO is no higher than 120 ppm.
4. The maximum heat removal duty of the heat exchange is $UA(T - T_w)$.
5. The upper limit of the *adiabatic end temperature* is $(T_b + 80)$°C.

Here, the threshold values on product quality are obtained from simulating the base case recipe, where the polymerization model is solved with the reaction time and controls fixed to their recipe values. Among them, UA and T_b are constant parameters that are specified according to the reactor configuration. The optimization problem is solved with GAMS/IPOPT to proved local optimality with appropriate initialization of the participating variables, and all computations are performed on a laptop with a quad-core 2.80GHz Intel®i7 processor and 6 GB memory, installed Linux kernel 3.2.0–14. Details on the statistics and solution of the model are tabulated in Table 2. Although the model size is large in terms of the number of variables and constraints, it can be solved within reasonable CPU time in minutes. The optimization model is initialized using the simulation result of the base case recipe. The optimal solution renders a batch processing time of 0.53 unit time, which is 47% less than the base case recipe. Meanwhile, the quality constraints on the product are satisfied at the end of the operation. It should be noted that the base case recipe and set of process constraints are chosen to illustrate the use of dynamic optimization and do not necessarily reflect the true capability or restrictions of the plant. Nevertheless, the actual potential reaction time saving is still significant.

The obtained optimal operating strategy is depicted in Figure 2. The optimized controls are shown in solid lines in comparison with the plant recipe in dashed lines. In the optimized scheme, the reactor temperature exhibits a U-shaped pattern: a high reactor temperature at the beginning period of operation can accelerate the hydrolysis and initiation reaction and, therefore, better *kick off* the following polymerization. And after that, the reactor temperature plunges down and stays low (lower than the corresponding recipe value) due to the process safety and product quality constraints. However, after the feeding period is over, the reactor temperature rises up for quick monomer digestion in the last few percent of the operation time horizon. The feed rate profile also starts at a high level, and gradually decreases during most of the operation time period. An important difference between the current plant recipe and the optimized one is that there are obviously two periods in the plant recipe: PO feeding followed by PO digestion. On the contrary, the optimized recipe tends to merge the two periods, and, therefore, the rising temperature at the end is needed to achieve the desired final level of PO. In Figure 3, we show the transition behavior of two critical constraining factors: the adiabatic end temperature and the heat removal rate. The adiabatic end temperature constraint is not active, since it does not reach the upper bound specified by $T_{ad} - T_b = 80$°C. The cooling capacity is the major limiting factor of the process, which stays active for most of the operation time horizon. The total capacity limit also includes a portion provided by the monomer feed. Note that here we assume the heat exchanger is not fouled, otherwise the optimal solution may drift. Considering heat exchanger fouling can bring

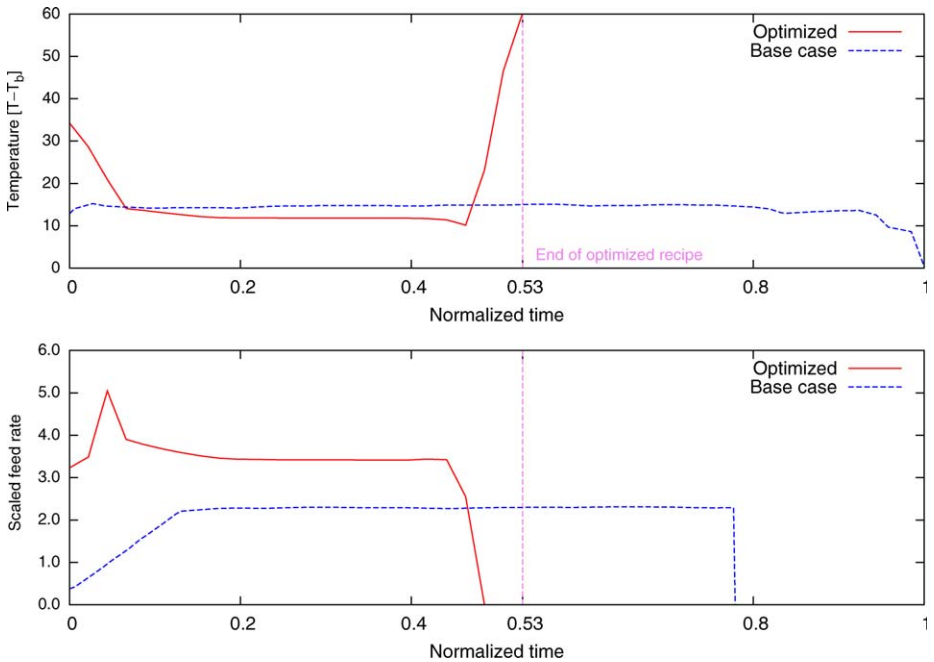

Figure 2. Optimal control profiles of the process.

[Color figure can be viewed in the online issue, which is available at wileyonlinelibrary.com.]

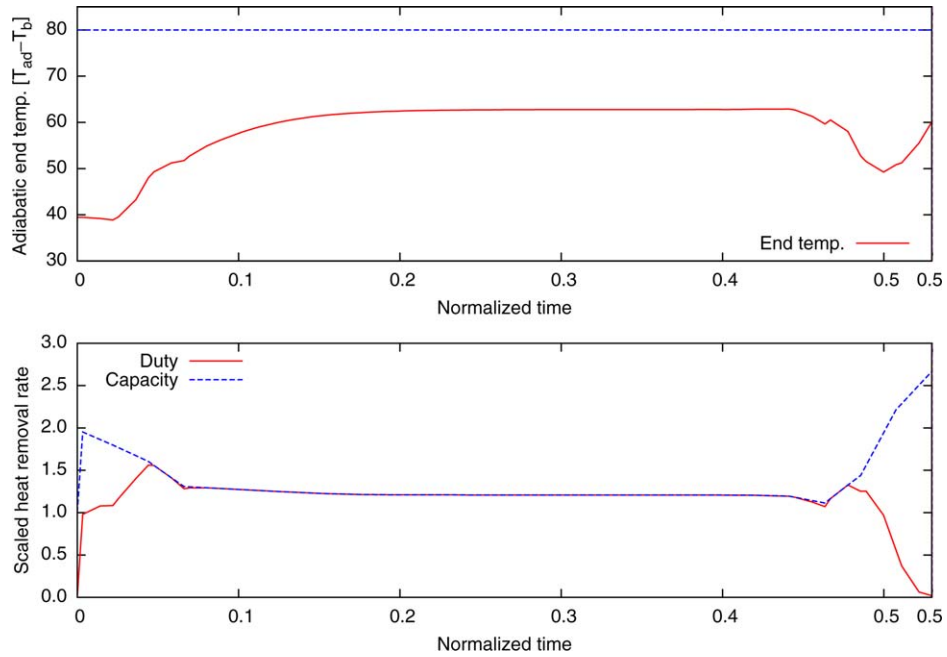

Figure 3. Process constraint profiles.

[Color figure can be viewed in the online issue, which is available at wileyonlinelibrary.com.]

additional complexity to the optimization problem,[9] and it remains an interesting future extension to our current work.

Figure 4 shows the population growth of the product and unsat polymer chains, where a number of species of particular chain lengths is presented. Note that the upper limit of 18 repeating units is admissible since the mole number of the longest chain stays close to zero for both types of polymers. During the polymerization, the monomers are continually added to the polymers and chains of higher lengths gradually appear and grow. A product chain of length n can either become length $n+1$ through the propagation reaction or transform into a dormant chain of equal length. It is also worth noting that the populations of the unsat chains sharply increase in the digestion period because of the rising reactor temperature. The final-time population distributions of the two polymers are given in histograms shown in Figure 5. The product polymer nearly follows the *Poisson* distribution, which agrees with the fact that the main population is nearly a well-defined living system. The maximum in the population is located at $n=7$, which is also the central position of the distribution. However, the distribution of the unsat chains significantly differs from the product, where the majority has less than 12 repeating units and the distribution follows in a descending manner from short chains to long ones, except

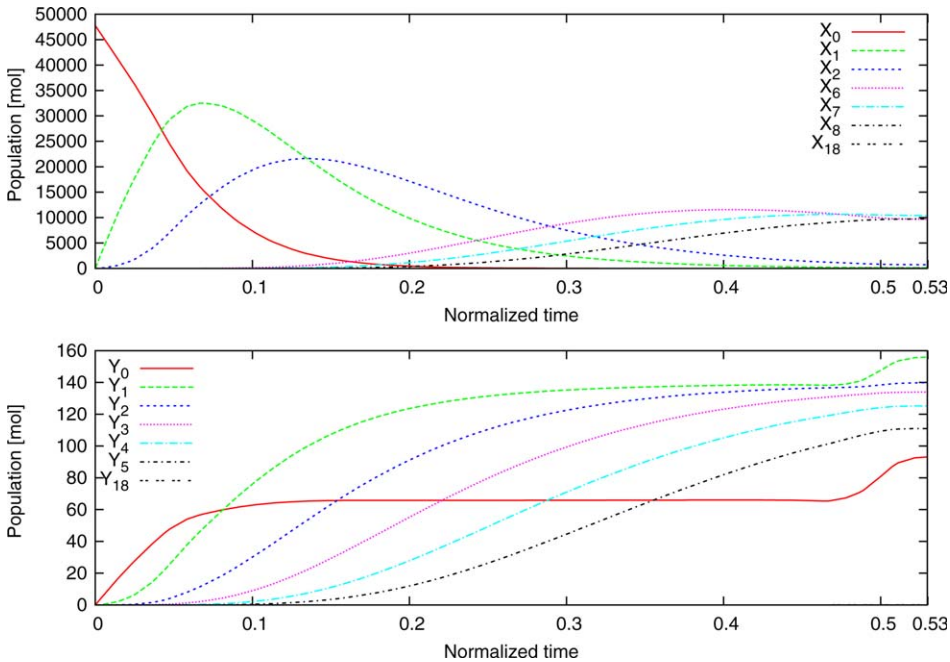

Figure 4. Population growth profiles of polymers of different chain lengths.

[Color figure can be viewed in the online issue, which is available at wileyonlinelibrary.com.]

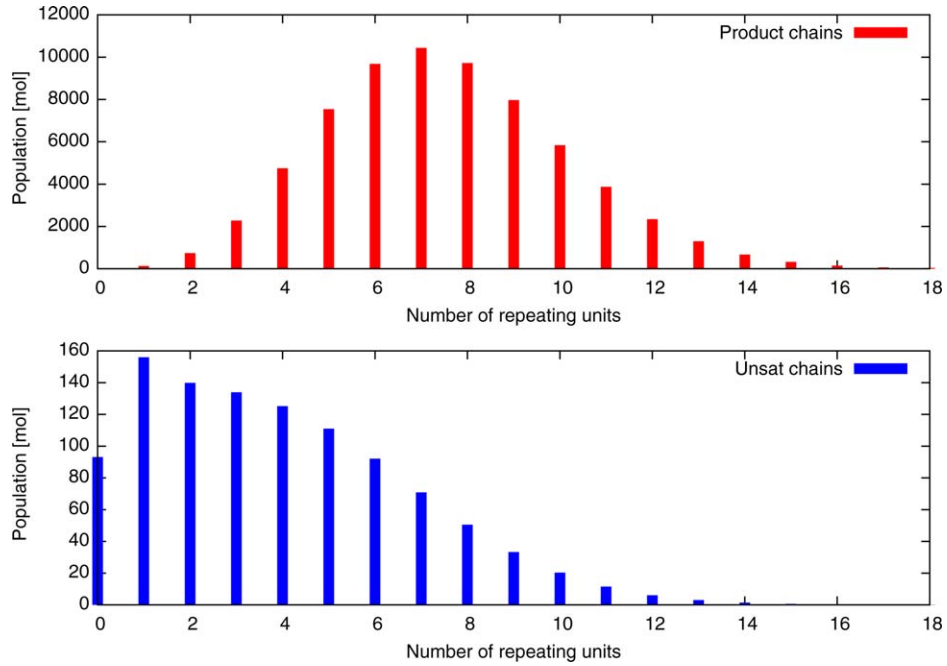

Figure 5. MW distributions in the final product.

[Color figure can be viewed in the online issue, which is available at wileyonlinelibrary.com.]

for the initiation chains $n = 0$, where the initiation reaction is faster than propagation. The MWD information is valuable for analyzing the product polyol properties, such as viscosity.

Figure 6 demonstrates the optimized number-average MWs and the PDI for both the product and the unsat (in solid lines), in comparison with the profiles obtained from the base case (in dashed lines). For the product chains, the optimized recipe reaches the same MW and PDI as the base case. But for the unsats, the PDI is higher for the optimized recipe while the MWs are very close in both cases. Note that the base case profiles show a time period in the end that has no significant changes in all quantities, but after optimization, those properties still change until the end of the batch. The number-average MW of the unsat chains is of the same

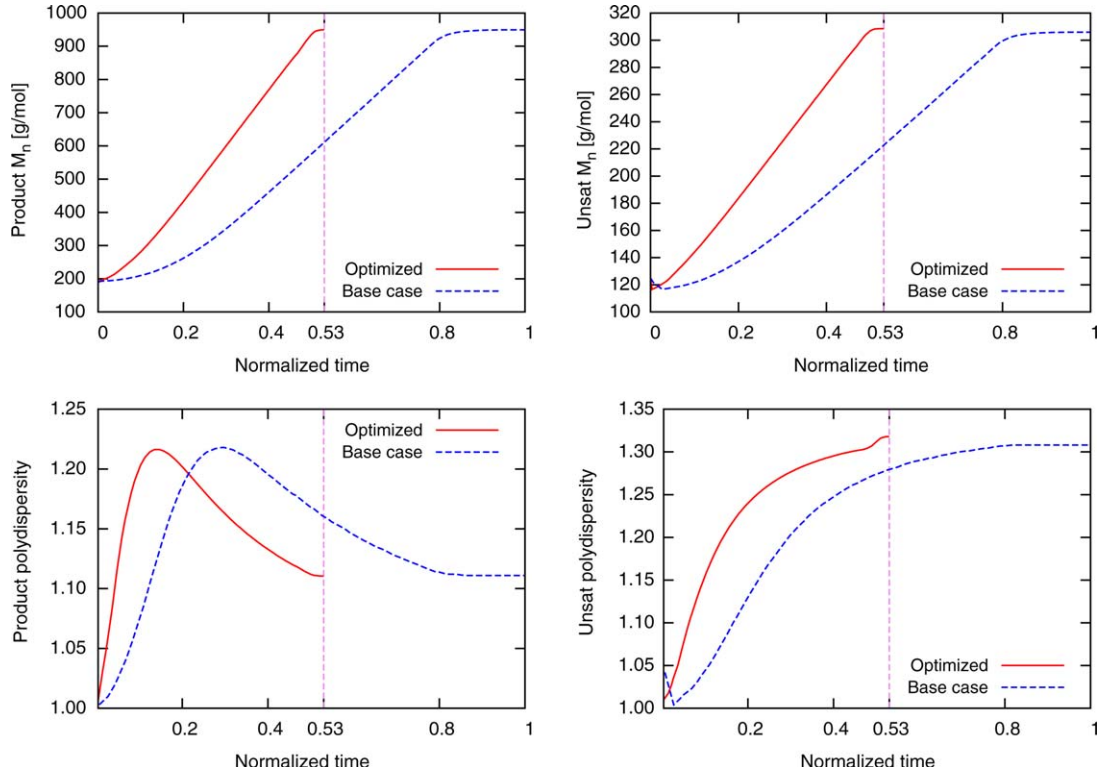

Figure 6. Polymer property profiles: MWs and polydispersity indices.

[Color figure can be viewed in the online issue, which is available at wileyonlinelibrary.com.]

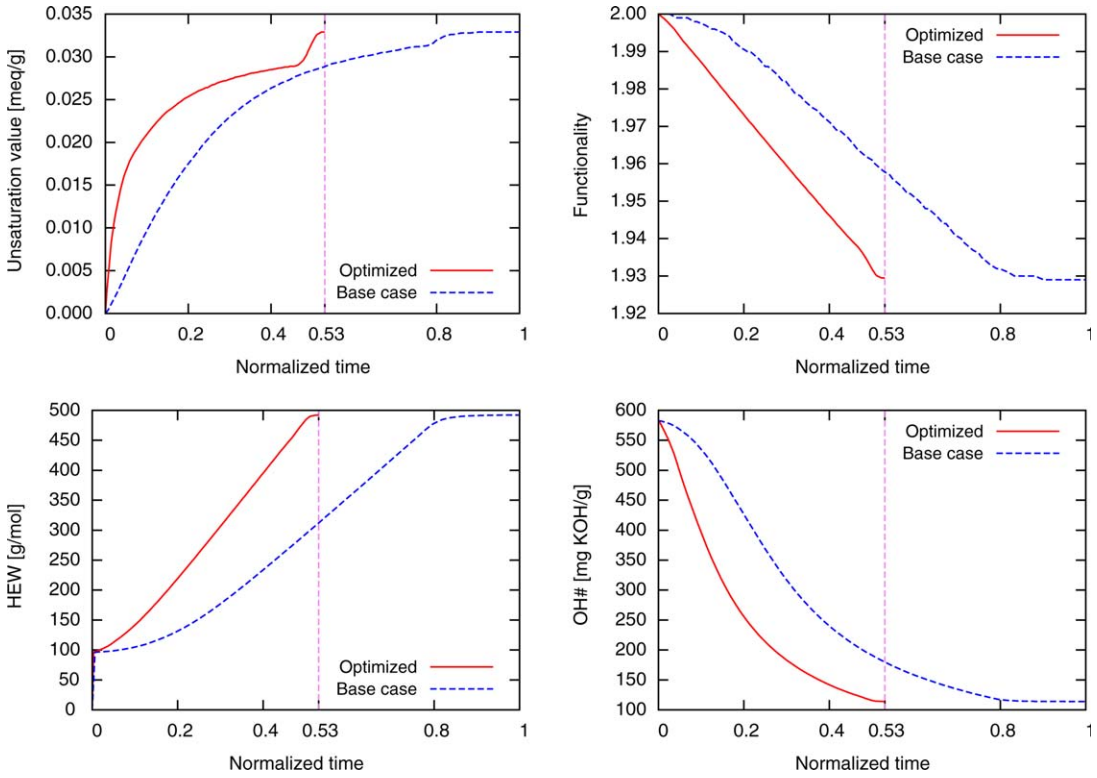

Figure 7. Polymer property profiles: important quality indices of polyols.

[Color figure can be viewed in the online issue, which is available at wileyonlinelibrary.com.]

order of magnitude of the product polymers. A large unsat number is particularly undesirable in this case, since it implies a considerable amount of monomer is consumed by the byproduct. In addition, the unsat chains have a larger PDI which indicates their distribution is more widely spread, agreeing with the distributions shown in Figure 5. Last, a group of commonly used quality indices are depicted in Figure 7. It can be concluded that their final-time values are in proper ranges.

Conclusions

In this article, we have addressed the reactor modeling and dynamic optimization of polyether polyol processes, using the production of polypropylene glycol as the example. The first-principles reactor model has been established through applying conservation laws, reaction kinetic relations, etc. and the original model demonstrated two-time-scale dynamic behaviors because of the presence of the fast cation-exchange reactions. Therefore, a reformulation procedure was conducted using the nullspace projection method, which aimed at separating the fast dynamic modes and modeling them as algebraic equations with regard to the quasi-steady states. The established model was validated against plant data using the reactor pressure profile. A number of key kinetic parameters from published literature have been adjusted during the model calibration process. Next, a dynamic optimization problem was formulated to improve the polymerization recipe design by minimizing the batch time. Several important limiting factors were introduced as the constraints in the optimization problem, concerning the product quality and process safety. To solve the optimization problem, we first translated the dynamic equations into nonlinear algebraic equations through the use of the simultaneous collocation method. This gave rise to a large-scale nonconvex NLP problem that we modeled and solved with GAMS and IPOPT. The study results illustrate detailed information on the dynamic characteristics of the polymerization process and show very promising performance of the optimized recipe by significantly reducing the required batch time. Particularly for the control design, the optimizer showed the trend to merge the feeding and digestion periods, which has changed the design pattern used for the base case recipe.

Acknowledgment

This contribution was identified by John Congalidis (E.I. du Pont de Nemours and Company) as the Best Presentation in the session "Modeling and Control of Polymer Processes" of the 2012 AIChE Annual Meeting in Pittsburgh, PA.

Notation

Notation used in the process model

a = liquid-phase activity, dimensionless
A = heat-transfer area, m^2
A_r = pre-exponential factor, m^3/mol s
c_p = specific heat capacity, J/g K
D = dormant product chains
E_r = activation energy, J/mol
f = functionality, dimensionless
F = monomer feed rate, mol/s
G = growing product chains
H = enthalpy, J/g
ΔH = reaction heat, J/g
k = reaction rate constant, m^3/mol s
l = number-average chain length, dimensionless
m = total mass, g
M = monomer

M_n = number-average molecular weight of polyol, g/mol
M_w = weight-average molecular weight of polyol, g/mol
MW = molecular weight, g/mol
n = number of moles, mol
N = maximum number of repeating units
P = pressure, kPa
q = heat removal rate, J/s
Q = growing unsat chains
r = reaction rate, mol/s
R = dormant unsat chains
R = universal gas constant, 8.314 J/mol K
t = time, s
T = temperature, K
T_{ad} = adiabatic end temperature, K
T_b = reference temperature, K
U = overall heat-transfer coefficient, W/m^2 K
V = liquid volume, m^3
$\bar{V}$ = gas volume, m^3
W = water
X = total product chains
Y = total unsat chains
γ = polymer moment, mol
ϕ = lattice fraction, dimensionless
χ = interaction parameter, dimensionless
$[\cdot]$ = concentration, mol/m^3

Subscripts

Substances

b = bulk
c = catalyst
f = feed
i = initiator
m = repeating units
n = repeating units
p = polymer
s = solvent
u = unsaturated chains
w = water

Reactions

h = hydrolysis
i = initiation
p = propagation
e = exchange
t = transfer

Notation used in the dynamic optimization formulation

h = length of finite elements, dimensionless
ℓ = Lagrange polynomial
K = maximum number of finite elements, dimensionless
t_f = final time, s
u = control variables
y = algebraic state variables
z = differential state variables
Ω = collocation coefficients, dimensionless
τ = normalized time, dimensionless

Subscripts

i = finite elements
j = collocation points

Literature Cited

1. Ionescu M. *Chemistry and Technology of Polyols for Polyurethanes*. Shropshire, UK: Smithers Rapra Technologies, 2005.
2. Herrington R, Hock K. *Dow Polyurethane Flexible Foams*. Midland, MI: Dow Chemical Co., 1997.
3. Guibert R, Plank C, Gerhard E. Kinetics of propylene oxide-oxypropylated glycerol reaction. *Ind Eng Chem Process Des Dev*. 1971;10:497–500.
4. Di Serio M, Tesser R, Dimiccoli A, Santacesaria E. Kinetics of ethoxylation and propoxylation of ethylene glycol catalyzed by KOH. *Ind Eng Chem Res*. 2002;41:5196–5206.
5. Simons D, Verbanc J. The polymerization of propylene oxide. *J Polym Sci*. 1960;44:303–311.
6. Yu G, Masters A, Heatley F, Booth C, Blease T. Anionic polymerisation of propylene oxide. Investigation of double-bond and head-to-head content by NMR spectroscopy. *Macromol Chem Phys*. 1994;195:1517–1538.
7. Wegener G, Brandt M, Duda L, Hofmann J, Klesczewski B, Koch D, Kumpf R, Orzesek H, Pirkl H, Six C, Steinlein C, Weisbeck M. Trends in industrial catalysis in the polyurethane industry. *Appl Catal A: Gen*. 2001;221:303–335.
8. Di Serio M, Tesser R, Santacesaria E. Comparison of different reactor types used in the manufacture of ethoxylated, propoxylated products. *Ind Eng Chem Res*. 2005;44:9482–9489.
9. Zavala V, Biegler L. Optimization-based strategies for the operation of low-density polyethylene tubular reactors: nonlinear model predictive control. *Comput Chem Eng*. 2009;33:1735–1746.
10. Flores-Tlacuahuac A, Biegler L, Saldívar-Guerra E. Dynamic optimization of HIPS open-loop unstable polymerization reactors. *Ind Eng Chem Res*. 2005;44:2659–2674.
11. Chatzidoukas C, Kiparissides C, Perkins J, Pistikopoulos E. Optimal grade transition campaign scheduling in a gas-phase polyolefin FBR using mixed integer dynamic optimization. *Comput Aid Chem Eng*. 2003;14:71–76.
12. Bonvin D, Bodizs L, Srinivasan B. Optimal grade transition for polyethylene reactors via NCO tracking. *Chem Eng Res Des*. 2005;83:692–697.
13. Zavala V, Flores-Tlacuahuac A, Vivaldo-Lima E. Dynamic optimization of a semi-batch reactor for polyurethane production. *Chem Eng Sci*. 2005;60:3061–3079.
14. Lin W, Biegler L, Jacobson A. Modeling and optimization of a seeded suspension polymerization process. *Chem Eng Sci*. 2010;65:4350–4362.
15. Feehery W, Barton P. Dynamic optimization with state variable path constraints. *Comput Chem Eng*. 1998;22:1241–1256.
16. Schlegel M, Stockmann K, Binder T, Marquardt W. Dynamic optimization using adaptive control vector parameterization. *Comput Chem Eng*. 2005;29:1731–1751.
17. Biegler L. *Nonlinear Programming: Concepts, Algorithms, and Applications to Chemical Processes*. Philadelphia, PA: Society for Industrial and Applied Mathematics, 2010.
18. Finlayson B. *The Method of Weighted Residuals and Variational Principles: With Application in Fluid Mechanics, Heat and Mass Transfer*. New York, NY: Academic Press, 1972.
19. Gee G, Higginson W, Taylor K, Trenholme M. The polymerization of epoxides. Part III. The polymerization of propylene oxide by sodium alkoxides. *J Chem Soc*. 1961;4298–4303.
20. Heatley F, Luo Y, Ding J, Mobbs R, Booth C. A carbon-13 nuclear magnetic resonance study of the triad sequence structure of block and statistical copolymers of ethylene oxide and propylene oxide. *Macromolecules*. 1988;21:2713–2721.
21. Hungenberg K. *Handbook of Polymer Reaction Engineering*. Wiley Online Library, New York, 2008.
22. Villa C. Reactor modeling for polymerization processes. *Ind Eng Chem Res*. 2007;46:5815–5823.
23. Gagnon S. *Polyethers, Propylene Oxide Polymers. Kirk-Othmer Encyclopedia of Chemical Technology*. New York, NY: Wiley, 2000.
24. Flory P. *Principles of Polymer Chemistry*. New York, NY: Cornell University Press, 1953.
25. Kumar A, Daoutidis P. Nonlinear dynamics and control of process systems with recycle. *J Process Control*. 2002;12:475–484.
26. Abel O, Marquardt W. Scenario-integrated modeling and optimization of dynamic systems. *AIChE J*. 2000;46:803–823.
27. Verwijs J, Papadopulos W, Weston J, Elwell R, Villa C. Continuous process and system of producing polyether polyols. US Patent App. 12/054,782, 2008.
28. Drud A. CONOPT—a large-scale GRG code. *INFORMS J Comput*. 1994;6:207.
29. Wächter A, Biegler L. On the implementation of an interior-point filter line-search algorithm for large-scale nonlinear programming. *Math Program*. 2006;106:25–57.
30. Brooke A, Kendrick D, Meeraus A, Raman R, Rosenthal R. *GAMS a User's Guide*. Washington, DC: GAMS Development Corporation, 2006.
31. Pantelides C, Renfro J. The online use of first-principles models in process operations: review, current status and future needs. *Comput Chem Eng*. 2013;51:136–148.
32. Bajorek S, Schnelle J. Identification and Experimental Database for Binary and Multicomponent Mixtures with Potential for Increasing Overall Cycle Efficiency. *Tech. rep*., Kansas State University, 2002.
33. Yaws C. *Yaws' Handbook of Thermodynamic and Physical Properties of Chemical Compounds*. 2003. Available at: http://www.knovel.com.
34. Beaumont R, Clegg B, Gee G, Herbert J, Marks D, Roberts R, Sims D. Heat capacities of propylene oxide and of some polymers of ethylene and propylene oxides. *Polymer*. 1966;7:401–417.

35. Yaws C, Narasimhan P, Gabbula C. Yaws' *Handbook of Antoine Coefficients for Vapor Pressure*, 2nd Electronic ed. 2009. Available at: http://www.knovel.com.
36. Stull D. Vapor pressure of pure substances. Organic and inorganic compounds. *Ind Eng Chem.* 1947;39:517–540.

Appendix A: Reformulation of the Propoxylation Model

The nullspace projection method is applied to reformulate the propoxylation model. First, the population balance equations involving the exchange reactions are converted into a matrix representation, and then the reformulation method can be systematically carried out.

Matrix representation of the model

For each adduct set, the population is defined as the product of its concentration and the liquid volume, that is

$$\mathrm{x}_n=[\mathrm{x}_n]V, \qquad x=\{\mathrm{G},\mathrm{D},\mathrm{Q},\mathrm{R}\}, n=0,1,\ldots,N \tag{A1}$$

Similar definitions can be introduced for the monomer (M) and water (W). According to the form in Eq. 24, the state vector can be defined as

$$\mathrm{x}^{\mathrm{T}}=\begin{bmatrix}\mathrm{W} & \mathrm{M} & \mathrm{G}^{\mathrm{T}} & \mathrm{D}^{\mathrm{T}} & \mathrm{Q}^{\mathrm{T}} & \mathrm{R}^{\mathrm{T}}\end{bmatrix} \tag{A2}$$

Here, G represents the vector of population $[\mathrm{G}_0 \quad \mathrm{G}_1 \quad \cdots \quad \mathrm{G}_N]^{\mathrm{T}}$, and similarly for the other polymeric species. Meanwhile, the reaction rate vector $r(\mathrm{x})$ consists of eight segments with regard to the hydrolysis reaction, as well as the initiation, propagation, transfer, and exchange reactions of both the normal and unsat chains. Mathematically, it reads

$$r^{\mathrm{T}}=\begin{bmatrix}r_1^{\mathrm{T}} & r_2^{\mathrm{T}} & \cdots & r_8^{\mathrm{T}}\end{bmatrix} \tag{A3a}$$

$$r_1=\begin{bmatrix}V^{-1}k_{\mathrm{h}}\mathrm{WM}\end{bmatrix} \tag{A3b}$$

$$r_2=\begin{bmatrix}V^{-1}k_{\mathrm{i}}\mathrm{G}_0\mathrm{M}\end{bmatrix} \tag{A3c}$$

$$r_3=\begin{bmatrix}V^{-1}k_{\mathrm{p}}\mathrm{G}_1\mathrm{M} & \cdots & V^{-1}k_{\mathrm{p}}\mathrm{G}_{N-1}\mathrm{M}\end{bmatrix}^{\mathrm{T}} \tag{A3d}$$

$$r_4=\begin{bmatrix}V^{-1}k_{\mathrm{i}}\mathrm{Q}_0\mathrm{M}\end{bmatrix} \tag{A3e}$$

$$r_5=\begin{bmatrix}V^{-1}k_{\mathrm{p}}\mathrm{Q}_1\mathrm{M} & \cdots & V^{-1}k_{\mathrm{p}}\mathrm{Q}_{N-1}\mathrm{M}\end{bmatrix}^{\mathrm{T}} \tag{A3f}$$

$$r_6=\begin{bmatrix}V^{-1}k_{\mathrm{t}}\mathrm{G}_0\mathrm{M} & \cdots & V^{-1}k_{\mathrm{t}}\mathrm{G}_N\mathrm{M}\end{bmatrix}^{\mathrm{T}} \tag{Ag}$$

$$r_7=\begin{bmatrix}V^{-1}k_{\mathrm{t}}\mathrm{Q}_0\mathrm{M} & \cdots & V^{-1}k_{\mathrm{t}}\mathrm{Q}_N\mathrm{M}\end{bmatrix}^{\mathrm{T}} \tag{A3h}$$

$$r_8=\begin{bmatrix}V^{-1}k_{\mathrm{e}}\mathrm{G}_n\mathrm{D}_m & V^{-1}k_{\mathrm{e}}\mathrm{G}_n\mathrm{R}_m & V^{-1}k_{\mathrm{e}}\mathrm{Q}_n\mathrm{D}_m & V^{-1}k_{\mathrm{e}}\mathrm{Q}_n\mathrm{R}_m\end{bmatrix}^{\mathrm{T}}, \quad n,m=0,1,\ldots,N \tag{A3i}$$

The equation system can be written in a comprehensive manner as shown below

$$\frac{d}{dt}\begin{bmatrix}\mathrm{W}\\ \mathrm{M}\\ \hline \mathrm{G}\\ \hline \mathrm{D}\\ \hline \mathrm{Q}\\ \hline \mathrm{R}\end{bmatrix}=\left[\begin{array}{c|c} A_{11} & \\ \hline A_{12} & \begin{array}{c} A_{21} \\ \hline -A_{21} \\ \hline A_{22} \\ \hline -A_{22} \end{array}\end{array}\right]\begin{bmatrix}r_1\\ r_2\\ \vdots\\ r_7\\ \hline r_8\end{bmatrix}+[B]F \tag{A4}$$

In the partitioned coefficient matrix, A_{11} corresponds to the reaction rates for water and monomers. For the polymers, A_{12} represents the nonequilibrium reaction coefficients, from r_1 to r_7; A_{21} includes the terms from the equilibrium (exchange) reactions for G, and the submatrix for D is $-A_{21}$ since the population of D changes reversely; similarly, A_{22} and $-A_{22}$ are defined for Q and R, respectively. The input matrix $B=[0 \quad 1 \quad 0 \quad \ldots \quad 0]^{\mathrm{T}}$ as the feed contains only the monomer.

Reformulated model

The particular structure of Eq. A4 allows us to define the range $\mathcal{Y}$ and the nullspace matrix $\mathcal{Z}$ as

$$[\mathcal{Y}\mid\mathcal{Z}]=\left[\begin{array}{cccc|cc} I_2 & & & & & \\ & I_{N+1} & & & I_{N+1} & \\ & -I_{N+1} & & & I_{N+1} & \\ & & I_{N+1} & & & I_{N+1} \\ & & -I_{N+1} & & & I_{N+1} \end{array}\right]. \tag{A5}$$

It can be verified that $\mathcal{Z}^{\mathrm{T}}A_2=0$, and the reformulated system is obtained as stated in Eqs. 16−18.

Appendix B: Model Parameters

Heat capacities for enthalpy calculations are listed in Table B1. The Antoine equation coefficients for vapor pressure

Table B1. Heat Capacity Coefficients

	A	B	C	D	Reference
Feed (f)	0.92	8.87×10^{-3}	-3.10×10^{-5}	4.78×10^{-8}	Yaws[33]
Bulk (b)	1.10	2.72×10^{-3}	0	0	Beaumont et al.[34]

$c_{pi}=A_i+B_iT+C_iT^2+D_iT^3, i=\{f,b\}$.

Table B2. Antoine Equation Coefficients

	A	B	C	Reference
Water	7.18	1723.64	−40.07	Yaws et al.[35]
PO	6.28	1158.00	−36.93	Yaws et al.[35]
PG	8.08	2692.19	−14.97	Stull[36]

Table B3. Kinetic Parameters of KOH Catalyzed Propoxylation

Model Parameter	Unit	Reference
$A_{\mathrm{h}}=240,420$	m^3/mol s	Di Serio et al.[4]
$E_{\mathrm{h}}=82,425$	J/mol	Di Serio et al.[4]
$A_{\mathrm{i}}=396,400$	m^3/mol s	Di Serio et al.[4]
$E_{\mathrm{i}}=77,822$	J/mol	Di Serio et al.[4]
$A_{\mathrm{p}}=8504$	m^3/mol s	Guibert et al.[3]
$E_{\mathrm{p}}=69,172$	J/mol	Guibert et al.[3]
$A_{\mathrm{t}}=950,410$	m^3/mol s	[a]
$E_{\mathrm{t}}=105,018$	J/mol	Gee et al.[19]
$(-\Delta H_{\mathrm{p}})=92,048$	J/mol	Herrington and Hock[2]

[a]Calculated by using $k_{\mathrm{p}}=800k_t$, when $T=105°\mathrm{C}$.

calculations are tabulated in Table B2. Other important parameters used are listed as below:

Universal gas constant	$R=8.314\text{J/mol}\quad\text{K}$
Initial amount of nitrogen	n_{N_2}
Maximum reactor pressure	$P^{\max}$
Total reactor volume	$V+\bar{V}$
Interaction parameter	χ (in the Flory-Huggins theory)
Liquid-phase activity of water	a_{H_2O}
Liquid-phase activity of propylene glycol	a_{PG}

The initial amount of nitrogen charged in the reactor, the maximum pressure and the reactor volume are given by the associated process specification. The interaction parameter is decided on our experience with the alkoxylation system. The liquid-phase activities of water and propylene glycol are obtained from the technical report.[32] These parameters are adjusted to match the pressure profile from plant data. Moreover, in Table B3, the kinetic constants are expressed with the Arrhenius temperature dependence $k_r=A_r\exp\left(-\frac{E_r}{RT}\right), r=\{h,i,p,t\}$. The parameter values are obtained from published literature as noted in the last column, and some of them are adjusted to fit the plant pressure profile in our case study.

Manuscript received Jan. 21, 2013, and revision received Apr. 2, 2013.